Astronomy & Astrophysics manuscript no. ms
March 22, 2010

New Baade-Wesselink distances and radii for four metal-rich Galactic Cepheids⋆

S. Pedicelli[1,2], B. Lemasle[3], M. Groenewegen[4], M. Romaniello[1], G. Bono[2,5], C. D. Laney,[6], P. François[7], R. Buonanno,[2,8], F. Caputo,[5], J. Lub,[9], J. W. Pel,[3], F. Primas[1], and J. Pritchard[1]

[1] European Southern Observatory (ESO) Karl-Schwarzschild-Strasse 2, D-85748 Garching bei München, Germany; e-mail: spedicel@eso.org
[2] Università di Roma Tor Vergata, Via della Ricerca Scientifica 1, 00133 Roma, Italy
[3] Kapteyn Institute, University of Groningen, P.O. Box 800, 9700 AV Groningen, The Netherlands
[4] Royal Observatory of Belgium, Ringlaan 3 B-1180 Brussels, Belgium
[5] INAF – Osservatorio Astronomico di Roma, Via Frascati 33, Monte Porzio Catone, Italy
[6] South African Astronomical Observatory, PO Box 9, 7935 Observatory, South Africa
[7] Observatoire de Paris-Meudon, GEPI, 61 avenue de l'Observatoire, F-75014 Paris, France
[8] ASI–Science Data Center, ASDC c/o ESRIN, via G. Galilei, 00044 Frascati, Italy
[9] Leiden Observatory, Leiden University, P.O. Box 9513, NL-2300 RA Leiden, The Netherlands

Received September 15, 1996; accepted March 16, 1997

ABSTRACT

Aims. We provided accurate estimates of distances, radii and iron abundances for four metal-rich Cepheids, namely V340 Ara, UZ Sct, AV Sgr and VY Sgr. The main aim of this investigation is to constrain their pulsation properties and their location across the Galactic inner disk.

Methods. We adopted new accurate NIR (J,H,K) light curves and new radial velocity measurements for the target Cepheids to determinate their distances and radii using the Baade-Wesselink technique. In particular, we adopted the most recent calibration of the IR surface brightness relation and of the projection factor. Moreover, we also provided accurate measurements of the iron abundance of the target Cepheids.

Results. Current distance estimates agree within one σ with similar distances based either on empirical or on theoretical NIR Period-Luminosity relations. However, the uncertainties of the Baade-Wesselink distances are on average a factor of 3-4 smaller when compared with errors affecting other distance determinations. Mean Baade-Wesselink radii also agree at one σ level with Cepheid radii based either on empirical or on theoretical Period-Radius relations. Iron abundances are, within one σ, similar to the iron contents provided by Andrievsky and collaborators, thus confirming the super metal-rich nature of the target Cepheids. We also found that the luminosity amplitudes of classical Cepheids, at odds with RR Lyrae stars, do not show a clear correlation with the metal-content. This circumstantial evidence appears to be the consequence of the Hertzsprung progression together with the dependence of the topology of the instability strip on metallicity, evolutionary effects and binaries.

Key words. Stars: radial velocity – Stars: distances – Cepheids

1. Introduction

Classical Cepheids are used both as standard candles and tracers of young stellar populations (Maciel & Costa 2009; Pedicelli et al. 2009). They are bright and variable objects and thanks to the Hubble Space Telescope they have been identified and accurately measured in Local Group ($d \lesssim 1$ Mpc) and in Local Volume ($d \lesssim 10$ Mpc) galaxies (Freedman et al. 2001; Tammann et al. 2003; Bono et al. 2008). They obey to a Period-Luminosity (PL) relation and are the most popular primary distance indicators (Feast 1999; Macri et al. 2006; Fouqué et al. 2007; Groenewegen 2007; di Benedetto 2008; Groenewegen 2008; Kervella et al. 2008; Kanbur et al. 2009; Marengo et al. 2009; Scowcroft et al. 2009). In spite of these outstanding observational and theoretical efforts (Marconi 2009, and references therein) the universality of optical and near-infrared (NIR) PL relations still lacks a firm empirical validation (Benedict et al. 2007; Romaniello et al. 2008; Sandage et al. 2009).

This thorny problem remains even if the zero-point and the slope of the PL relation can be estimated with a variety of independent methods. Ideally the calibration and the validation of the PL relation should be rooted on distances measured with a geometrical method such as the trigonometric parallaxes. This approach was recently adopted by Benedict et al. (2007) who provided parallaxes with a mean accuracy of 8% for a sample of nine Galactic Cepheids using the *Fine Guidance Sensor* (FGS) on board of the Hubble Space Telescope (HST). A new revision of HIPPARCOS parallaxes for Galactic Cepheids (244 objects) has been recently provided by van Leeuwen (2007) and by van Leeuwen et al. (2007). The accuracy of the new measurements is on average a factor of two better than the old ones. However, the Cepheids with the most accurate HIPPARCOS parallaxes are Polaris (α UMa) and the prototype δ Cep. The accuracy of the former one is 1.6% (van Leeuwen et al. 2007), while the latter is similar to the accuracy of the FGS@HST parallax, namely 5.2% versus 4.1% (Mérand et al. 2005).

⋆ Based on observations made with MPG/ESO 2.2m telescope at La Silla Observatory under proposal IDs: 75.D-0676, 60.A-9120 and multi-epoch, multi-band NIR data at SAAO.

The Baade-Wesselink method (BW, Baade (1926); Wesselink (1946)) provides an independent empirical approach to measure Cepheid absolute distances and it can be applied to variable stars. This method relies on two observables: the radial velocity (v_r) and the variation of the angular diameter (θ). The latter parameter was historically substituted by the variation in color along the pulsation cycle. However, direct measurements of the Cepheid angular diameter have been recently provided by Kervella et al. (2004b) using the Very Large Telescope Interferometer (VLTI). In particular, the use of VLT INterferometer Commissioning Instrument (VINCI) gave the unique opportunity to provide angular diameter measurements along the pulsation cycle for seven Cepheids. These pioneer measurements encouraged a detailed comparison between theory and observations concerning the limb darkening and the atmosphere of variable stars (Marengo et al. 2003; Nardetto et al. 2007), but the number of Cepheids for which these measurements are available is still very limited.

To overcome the difficulties in the interferometric measurement of the angular diameter several variants of the BW method were suggested in the literature. Among them the methods based on the Surface-Brightness (SB) relations link variations in color with variations in angular diameters. This method can be applied to Cepheids for which accurate radial velocities and multi-wavelength light curves are available. Storm et al. (2004), Kervella et al. (2004a) and Groenewegen (2007) (hereafter G07) derived such relations, using an optical-NIR (V-K) color (IRSB), which gives the highest precision in the derived quantities.

However, the most relevant limit of the currently adopted BW methods is the value of the projection factor (p-factor). This parameter links radial velocity changes to radius changes and still lacks firm theoretical and empirical constraints (Nardetto et al. 2009). It can be empirically estimated using Cepheids for which accurate interferometric angular diameter measurements, radial velocity curves and trigonometric parallaxes are available. This approach was applied to δ Cep by Mérand et al. (2005) using the new optical interferometric measurements obtained with the CHARA Array, the FGS@HST trigonometric parallax by Benedict et al. (2007) and the radial velocities available in the literature. The p-factor they found – p=1.27 ± 0.06– agrees quite well with theoretical predictions by Nardetto et al. (2004). More recently, G07 found that the use of a constant p-factor (p=1.27 ± 0.05) for six Galactic Cepheids, with interferometrically measured angular diameter variations and known distances, agrees quite well with HST parallaxes. Moreover, he found that a strong period dependence of the p-factor ($p \sim -0.15 \cdot \log P$, Gieren et al. (2005)), could also be ruled out. However, a moderate period dependence ($p \sim -0.03 \cdot \log P$) as suggested either by Gieren et al. (1993, 1997, 1998); Barnes et al. (2003); Storm et al. (2004), or more recently by Nardetto et al. (2009) ($p \sim -0.08 \cdot \log P$) is still consistent with currently available data (G07).

In this investigation we plan to apply the BW method using the most recent calibration of the IRSB relation (Groenewegen 2010, hereinafter G10, in preparation), to estimate the distance of four metal-rich Galactic Cepheids. In particular, we plan to use new radial velocity measurements, new accurate NIR (J,H,K) light curves and V-band light curves available in the literature (Berdnikov 1992). Moreover, we discuss in §4 the iron abundance of the four target Cepheids using Fe I and Fe II lines. §5 deals with the pulsation amplitude of metal-rich Cepheids, while in §6 we summarize current findings and outline future developments of this project.

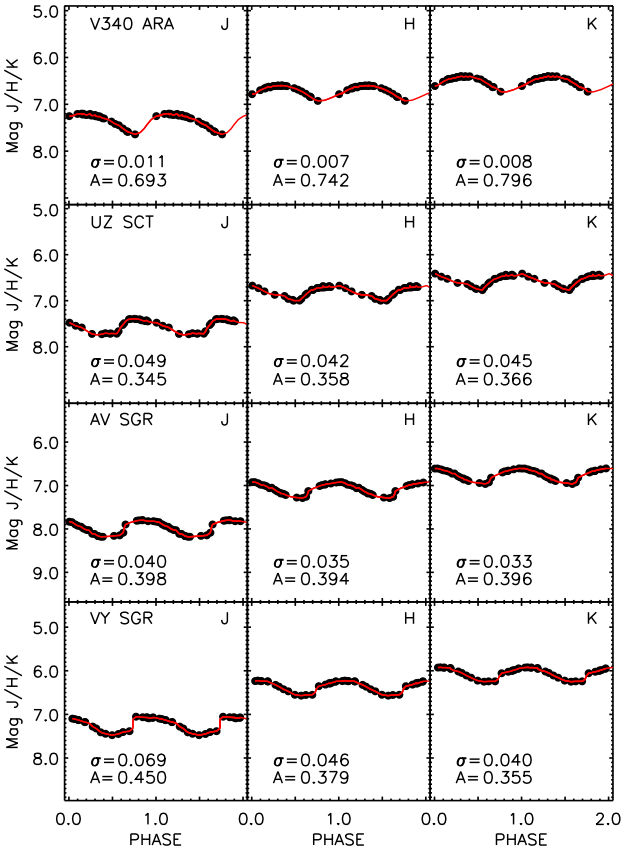

Fig. 1. From left to right J,H,K-band light curves for the four metal-rich selected Cepheids. In each panel are also plotted the intrinsic scatter (σ) of the fit with a cubic spline (red line) and the luminosity amplitude.

2. Photometric and spectroscopic data

The selected stars are the most metal-rich Cepheids in the large sample (113 objects) collected by Andrievsky et al. (2002a,b,c, 2004). Positional and physical parameters for the selected Cepheids are listed in Table 1.

2.1. Optical and NIR data

In order to provide accurate estimates of their distances we plan to use the most recent calibration of the IRSB relation (Barnes et al. 1976; Laney & Stobie 1995; Fouqué & Gieren 1997; Storm et al. 2004, G10). To accomplish this goal one of us (CDL) collected accurate multi-epoch, multi-band NIR data at SAAO for the four targets. The typical uncertainty of individual phase points ranges from 0.005 to 0.007 mag for $K < 6$ mag, deteriorating to about 0.012 at $K = 8.6$ mag. Figure 1 shows the J, H and K-band light curves for the target Cepheids. The intrinsic scatter (σ) of the fit with a cubic spline (red line) and the luminosity amplitude are also labeled. The mean NIR (J,H,K) magnitudes have been estimated as a time average on magnitudes and are listed in Table 1. The typical uncertainties are of the order of a few hundredths of a magnitude.

For three out of the four targets (AV Sgr, UZ Sct, VY Sgr) we have detailed optical light curves collected in the Walraven bands (Walraven et al. 1964; Lub & Pel 1975; Pel 1976; Lub & Pel 1977). However, for the Baade-Wesselink solution we decided to use more recent V-band light curves available

Table 1. Intrinsic parameters, mean NIR magnitudes and mean radial velocities for the target Cepheids.

NAME	α(J2000)[a]	δ(J2000)[a]	log P	E(B-V)[b]	$< J >^c \pm\sigma(J)$	$< H >^c \pm\sigma(H)$	$< K >^c \pm\sigma(K)$	N_s^d	$< v_r >^e$	Δv_r^e
V340 Ara	16 45 19	-51 20 33	1.32	0.574	7.382±0.011	6.809±0.007	6.619±0.008	25+2	-80.8±1.2	59.1
UZ Sct	18 31 22	-12 55 00	1.17	1.071	7.502±0.049	6.818±0.042	6.564±0.045	25+2	40.2±0.5	49.4
AV Sgr	18 04 49	-22 43 00	1.19	1.267	6.909±0.040	6.081±0.035	5.758±0.033	25+1	19.3±1.8	59.3
VY Sgr	18 12 05	-20 42 00	1.13	1.283	7.174±0.069	6.375±0.046	6.068±0.040	25+2	16.0±1.8	59.2

[a] Cepheid coordinates: units of right ascension are hours, minutes, and seconds; units of declination are degrees, arcminutes and arcseconds.
[b] Reddening according to Fernie et al. (1995).
[c] Mean NIR magnitudes.
[d] Number of spectra collected with FEROS at the 2.2m MPG/ESO telescope.
[e] Mean radial velocity and velocity amplitude (km s^{-1}).

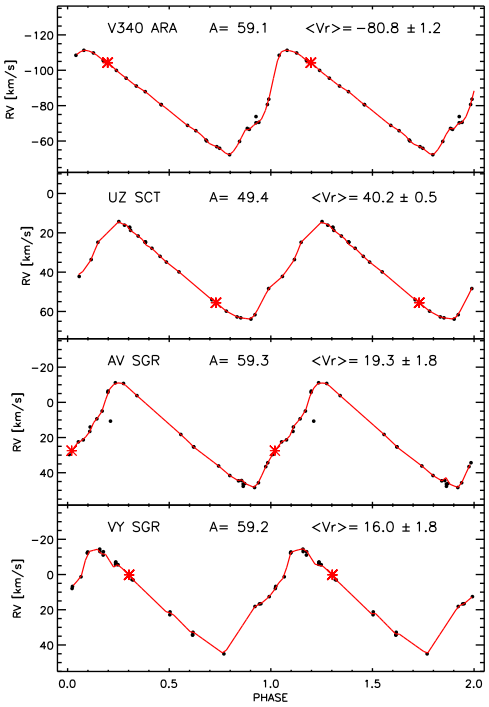

Fig. 2. Radial velocity curves for the four selected Cepheids, measured by cross-correlating a line list (see text). The red asterisks display the radial velocities based on the high S/N spectra adopted for measuring the iron abundance. The amplitude and the mean radial velocity (kms^{-1}) are labeled.

in the literature (Berdnikov 1992), since the accuracy improves if photometric and radial velocity data are collected close in time. The large sample of Cepheids with Walraven photometry will be used in Section 5, where we discuss the period-amplitude diagram.

2.2. Spectroscopic data

Together with photometric data we also secured for the target Cepheids accurate multi-epoch, high-resolution (R~30,000) spectra covering the entire pulsational cycle with FEROS@2.2m MPG/ESO telescope. The goal was to provide individual radial velocity measurements with an accuracy of 1 km/s for ≈ two dozen of epochs. The number of epochs is a strong requirement to reach with BW methods the nominal accuracy of 5% in distance. The spectroscopic sample, indeed, includes more than 25 spectra per Cepheid (see column 9 in Table 1). These spectra

Table 2. New weak Fe II line list added to the Fe I and Fe II line list of Romaniello et al. (2008).

λ[Å]	*Ion*	*EP*	log g_f
4893.82	Fe II	2.83	-4.45
4923.93	Fe II	2.88	-1.35
4993.35	Fe II	2.81	-3.56
5100.66	Fe II	2.81	-4.16
5132.67	Fe II	2.81	-3.95
5197.58	Fe II	3.23	-2.23
5234.63	Fe II	3.22	-2.22
5256.94	Fe II	2.89	-4.25
5325.56	Fe II	3.22	-3.18
5414.07	Fe II	3.22	-3.54
5425.26	Fe II	3.2	-3.27
5534.85	Fe II	3.24	-2.75
5932.06	Fe II	3.2	-4.81
7135.02	Fe II	6.21	-2.60
7301.56	Fe II	3.89	-3.68
7310.22	Fe II	3.89	-3.36
7672.37	Fe II	3.15	-5.19
7777.11	Fe II	3.20	-5.24
7801.24	Fe II	5.91	-2.94
7841.39	Fe II	3.90	-3.72
8250.34	Fe II	5.22	-3.29
8264.72	Fe II	6.81	-2.08
8324.96	Fe II	6.22	-2.75
8330.59	Fe II	6.22	-2.35
8490.08	Fe II	9.74	0.34
8981.13	Fe II	6.72	-2.18
8990.39	Fe II	6.23	-2.38
9095.11	Fe II	9.65	0.27
9122.92	Fe II	9.85	0.53
9132.37	Fe II	9.85	0.51
9187.16	Fe II	9.70	0.25
9244.74	Fe II	6.22	-2.40
9297.27	Fe II	9.65	0.41
9464.88	Fe II	6.09	-2.54
9572.60	Fe II	5.82	-2.87
9843.19	Fe II	6.14	-2.60
9849.74	Fe II	6.73	-2.30
9956.31	Fe II	5.48	-2.95

were collected between May and September 2005. The typical exposure time is ∼ 320s and the quality of the individual spectra is quite good (signal-to-noise ratio, $S/N \sim 70$) and allowed us to reach the required accuracy in radial velocity measurements. Radial velocity measurements were performed using `fitline` a semi-interactive routine developed by one of us (PF, François et al. (2007)). The algorithm adopted in `fitline` is

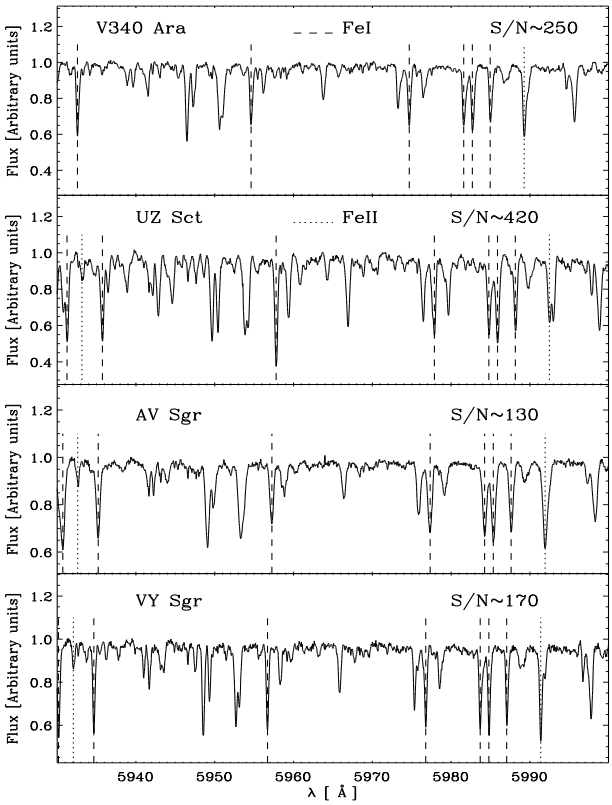

Fig. 3. High S/N spectra for the four selected Cepheids in a limited wavelength range (5930-6000 Å). Vertical dashed and dotted lines mark Fe I and Fe II lines. In each panel is also plotted the S/N ratio of either individual (AV Sgr) or co-added spectra.

based on a cross–correlation between the lines of each spectrum and a given line list. The reader interested in a more detailed description of `fitline` is referred to Lemasle et al. (2007, 2008). Note that to properly deal with metal-rich Cepheids the iron line list provided by Romaniello et al. (2008) was supplemented with three dozen of weak Fe II lines (see Table 2). Figure 2 shows the individual radial velocity measurements and the fit with a cubic spline (red lines). The mean radial velocities ($< v_r >$) and the velocity amplitudes (Δv_r) based on the spline fit are also labeled (see also columns 10 and 11 of Table 1).

The target Cepheids are among the most metal-rich Galactic Cepheids and, as expected, they are located close to the inner edge of the thin disk (Pedicelli et al. 2009). In order to provide accurate iron abundance measurements, we also collected for each target 1-2 high S/N ratio spectra with FEROS@2.2m MPG/ESO telescope (see red asterisks in Figure 2 and Table 1). These spectra were collected by one of us (PF) at the end of March 2007. The typical exposure time is $\sim$ 1800s and their S/N ratio ranges from 150 to 300. The abundance analysis of the Cepheids with two high S/N spectra was performed on the co-added spectrum, since they were collected close in time. Figure 3 shows the co-added spectra for the four selected Cepheids in the wavelength range between 5930 and 6000 Å. The vertical dashed and dotted lines mark Fe I (λ=5930.17, 5934.66, 5956.70, 5976.78, 5983.69, 5984.79, 5987.05 Å) and Fe II (λ=5932.06, 5991.37 Å) lines, respectively. The S/N ratio of either individual (AV Sgr) or co-added spectra is also labeled.

3. BW method

The BW method adopted to estimate distances and radii has already been discussed in previous papers by Groenewegen (Groenewegen 2004, 2007, 2008). In the following we briefly mention the key points of the method and the differences with the original approach. According to the definition of quasi-monochromatic surface brightness, we can write M_V - S_V + $5\times \log(R/R_\odot)$ = const. The absolute magnitude, and in turn the distance, can be found by differentiating this equation with respect to the pulsation phase, by multiplying the result for a color index $-(V-K)_0-$ and then by integrating over the entire pulsation cycle. The radial velocity is tightly connected with the pulsation velocity and the curve can be integrated to obtain the radius variation as a function of time (phase):

$$\Delta R(t,\delta\theta) = -p\int_{t_0}^{t+P\delta\theta}(v_r(t)-v_\gamma)dt \quad (1)$$

where P is the pulsation period, p the projection factor, v_γ the systematic radial velocity and $\delta\theta$ accounts for a phase shift between the radial velocity curve and the angular diameter changes measured either interferometrically or via the SB relation. Eventually, we end up with the equation $\Theta(t)$= const.$\times$ $[R_0 + \Delta R(t,\delta\theta)]/d$ where $\Theta(t)$ is the angular diameter in mas, R_0 is stellar radius in solar radii and d the distance in parsec. We measure the apparent radial velocity v_r, i.e. the Doppler shift of absorption lines in the stellar atmosphere, projected along the line of sight and integrated over the stellar disk. To obtain the pulsational velocity we use the p-factor (see column 2 in Table 3) coming from Nardetto et al. (2009):

$$p = 1.31 \pm 0.06 - 0.08 \pm 0.05 \cdot \log(P) \quad (2)$$

Integration of the pulsational velocity over the entire pulsation cycle provides an estimate of the linear radius variation. The angular diameter variation was derived using the IRSB method and the $(V-K)$ color. The calibration adopted in this investigation was derived by G10:

$$\log\theta_0 = 0.2692\ (V-K)_0 + 0.5298 \quad (3)$$

The above relation together with the Eq. 1 gives, once integrated over the pulsation cycle, individual Cepheid distances.

3.1. Cepheid distances

Figure 4 shows from left to right the application of the BW method to V340 Ara, UZ Sct, AV Sgr and VY Sgr. For each Cepheid we plot the variation of the angular diameter against phase (bottom panels) and the change in angular diameter derived from the IRSB relation (see Eq. 3) against the change in radius (top panels) obtained by integration of the *RV* curve (see Eq. 1). The absolute magnitudes have been derived in a self-consistent way from the Fourier fit to the data. Note that the fit in the phase interval 0.8-1.0 is often poor. This limitation of the BW method was known before (Storm et al. 2004). It was argued that non-LTE effects and an increase in the micro turbulence during these phases may change the atmospheric structure, and in turn hamper the use of a simple surface-brightness relation (Bersier et al. 1997). Table 3 lists the estimated distances and radii and the comparison with previous estimates. The errors listed in columns 3 and 4 of Table 3 give the uncertainties (one σ) on distance and radius for the target Cepheids. They account not only for the errors in the fit, but also for the errors estimated running several Monte Carlo simulations by artificially changing individual errors on V, K and RV measurements. In order

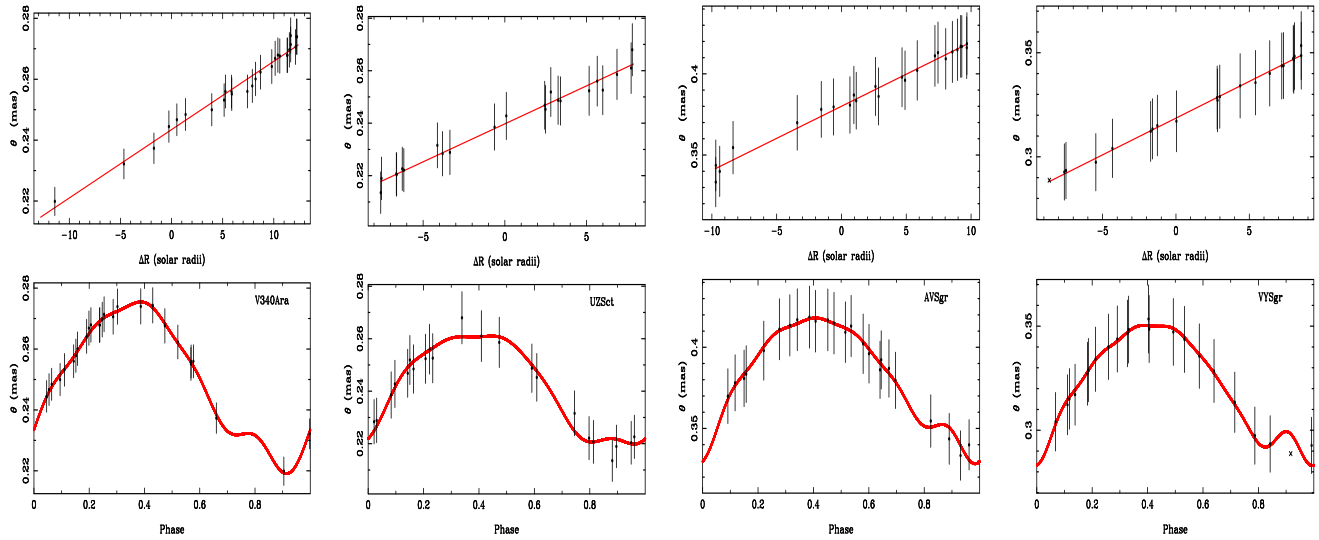

Fig. 4. From left to right: V340 Ara, UZ Sct, AV Sgr and VY Sgr. For each star, the top panels show the linear-bisector fit to the angular diameter as a function of radial displacement. The bottom panels show the angular diameter against phase. Crosses mark data-points not included in the fit.

to compare the above distances with similar estimates available in the literature we adopted the J, H and K-band PL relations for Galactic Cepheids recently provided by Fouqué et al. (2007). The mean of the three individual distances together with their errors for the target Cepheids are listed in column 5 of Table 3. The errors account for the uncertainty on the mean magnitudes and on the PL relations. The comparison indicates that distances based on the BW method and on NIR PL relation agree within 1σ. Current uncertainties on the BW distances, by taking into account the errors in the fit and the errors estimated using the Monte Carlo simulations, range from 6% (UZ Sct, AV Sgr, VY Sgr) to 14% (V340 Ara), while the uncertainties on the distances based on the empirical NIR PL relations range from 22% to 34%.

The NIR PL relations provided by Fouqué et al. (2007) do not account for a possible dependence of the NIR PL relation on the metal content. We are dealing with Cepheids characterized by super-solar iron abundances. Therefore, we estimated the Cepheid distances using theoretical NIR PL relations including both metal-intermediate and metal-rich Cepheid models (F. Caputo, private communication). Data listed in column 6 of Table 3 show that distances based on these theoretical NIR PL relations also agree within 1σ with the BW estimates. Note that the distances and their uncertainties based on theoretical PL relations are larger than the empirical ones, since the former relations were derived including all the fundamental models with abundances ranging from $Z = 0.001$ to $Z = 0.04$ and different helium contents (Bono et al. 2010, in preparation).

The mean Cepheid radii listed in column 4 of Table 3 agree quite well with mean radii based on empirical Period-Radius (PR) relation for Galactic Cepheids recently provided by G07 (see column 7 in Table 3). Note that this PR relation is based on six Galactic Cepheids with known distances (Benedict et al. 2007) and with interferometrically measured angular diameter variations (Kervella et al. 2004b; Mérand et al. 2005). The same outcome applies in the comparison with radii based on the predicted PR relation for Galactic Cepheids provided by Petroni et al. (2003), assuming a solar chemical composition. Current radii agree on average within 10% (two σ) with predicted and empirical PR relations.

4. Cepheid iron abundances

To measure the iron abundances of the target Cepheids we followed the same approach suggested by Lemasle et al. (2007). This approach relies on three different steps:

- **Line list**: The line list adopted by Romaniello et al. (2008), includes 275 Fe I lines and 37 Fe II lines covering the FEROS spectral range. However, the target Cepheids are metal-rich and a good fraction of Fe II are saturated. In order to provide robust estimates of intrinsic parameters and in turn accurate measurements of iron abundances, we supplemented the line list by Romaniello et al. (2008) with 39 new weak Fe II lines (see Table 2).
- **Equivalent width**: The measurement of the equivalent widths (EW) of the iron lines was performed using `fitline`. This code uses a Gaussian fit, which is defined by four parameters: central wavelength, width, depth and continuum value of the individual lines. The initial value of the Gaussian parameters is fixed by randomly selecting the four parameters. Then, the "genetic" algorithm computes the χ^2 between the observed line and the expected Gaussian profile and computes the new set of Gaussian parameters among the 20 best fit solutions of the previous "generation" by applying random modifications of the values of the parameters ("mutation"). The algorithm after 100-200 "generations", gives the best fit Gaussian parameters (lowest χ^2) for each observed line. For the measurement of the iron abundance, we have selected only lines with equivalent widths between 10 and 200 mÅ. The lower limit was chosen to be a safe compromise between the spectral characteristics and the need for weak lines for an optimal abundance determination. The upper limit was fixed to avoid the saturated portion of the curve of growth.
- **Stellar Parameters**: The determination of an accurate effective temperature is a critical point in the abundance determination. This requirement becomes even more important if we are dealing with variable stars, since the temperature estimate has to refer to the pulsation phase at which the spectrum was collected. In this analysis, the effective temperature

Table 3. Distances and radii according to the BW-analysis of the four selected Cepheids.

Name	p	d(pc)	$R/R_\odot$	$d(\mathrm{pc})^a_{PL}$	$d(\mathrm{pc})^b_{PL}$	$(R/R_\odot)^b_{G07}$	$(R/R_\odot)^c_{theo}$
V340 Ara	1.205	3890±126±547	100.2±3.2±17.3	3154±686	3754±1156	109.5±1.1	115±1
UZ Sct	1.217	3176±116±152	82.1±3.0±3.5	3117±871	3540±1177	86.4±1.1	91±1
AV Sgr	1.215	2302± 72±123	93.4±2.9±4.2	3036±792	3326±1063	89.2±1.1	94±1
VY Sgr	1.219	2546± 53±134	86.5±1.8±3.9	2300±663	2533± 849	81.1±1.1	86±1

[a] Mean *JHK*-distances based on empirical NIR PL relations (Fouqué et al. 2007).
[b] Mean *JHK*-distances based on theoretical NIR PL relations (Caputo, private communication).
[c] Radius estimate according to the empirical PR relation by G07.
[d] Radius estimate according to the theoretical PR relation by Petroni et al. (2003).

($T_{\rm eff}$) was estimated spectroscopically using the line depth ratios (LDR) method described in Kovtyukh & Gorlova (2000). This technique has the advantage of being independent of interstellar reddening and minimally dependent on metallicity. These uncertainties plague other methods like the integrated flux method or the color-temperature relations (Gray 1994; Krockenberger et al. 1998). This approach becomes even more relevant for the target Cepheids, since they are located close to the edge of the inner Galactic disk, and therefore they are characterized by high reddening values (see column 5 in Table 1). The estimated effective temperatures together with their errors are listed in columns 2 of Table 4. The surface gravity (log g) and the microturbulent velocity ($v_{\rm t}$) were constrained by minimizing the log([Fe/H]) vs. EW slope (using the Fe I abundance) and by imposing the ionization balance between Fe I and Fe II (see column 3 and 4 in Table 4). These two procedures are tightly connected and require an iterative process. The initial values for the microturbulent velocity and the surface gravity, were fixed using typical Cepheid values ($v_{\rm t}$=3 *km* s^{-1}, log g=2, Andrievsky et al. (2002b)). For the ionization balance, we assume that it was fulfilled when the difference between [Fe I/H] and [Fe II/H] was smaller than the standard deviation on [Fe II/H] (typically, $\sigma_{[Fe/H]} \sim 0.08 - 0.1$ dex). If this condition was satisfied by more than one value of log g, we checked which value satisfies also the ionization balance within the standard deviation on [Fe I/H] (typically, $\sigma_{[Fe/H]} \sim 0.02$ dex). The effective temperatures listed in column 5 ($T_{\rm eff}$(Model)) are the final best fit values of the atmosphere models adopted in the iterative process. To determine the errors on the microturbulent velocity and the surface gravity, we ran several iterations for each star, slightly modifying the values of these two intrinsic parameters that fulfill the requirements mentioned above. We have estimated that the intrinsic error on the microturbulent velocity is of the order of 0.1 *km* s^{-1}, while the intrinsic error on the surface gravity is of the order of 0.10 dex.

Our final Fe I and Fe II abundances, together with the adopted stellar parameters, are listed in Table 4. Data listed in column 8 of this table indicate that the mean iron contents have weighted intrinsic uncertainties of the order of 0.20 dex, due to errors in the EW measurements, in the intrinsic parameters and in the number of unsaturated iron lines. This finding further supports the difficulty in measuring the iron abundance of metal-rich Cepheids. The intrinsic accuracy can be certainly improved using high S/N ratio, multi-epoch spectra of the same targets, since empirical evidence suggests that Cepheid elemental abundances minimally depend on the pulsation phase (Luck & Andrievsky 2004; Kovtyukh et al. 2005). Finally, it is worth mentioning that

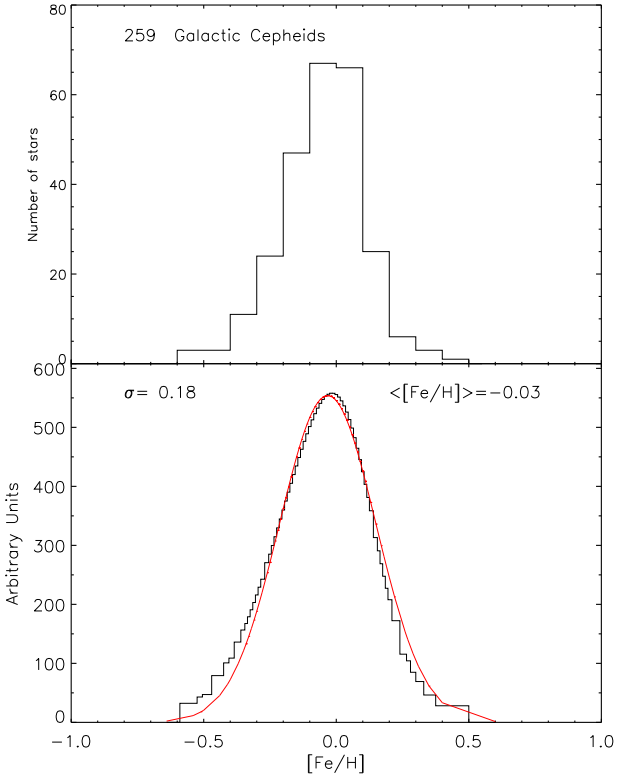

Fig. 5. Top – Metallicity distribution of Galactic Cepheids. Bottom – Same as the top, but the metallicity distribution was smoothed using a Gaussian kernel with standard deviation equal to the metallicity uncertainty of individual Cepheids. The red line shows the Gaussian fit of the metallicity distribution. The mean and the σ are also labeled.

current iron abundances agree, within one σ, with the abundances provided by Andrievsky et al. (2002b) using a similar approach (see last column in Table 4).

5. Period-Amplitude diagram

The metal-rich regime of classical Cepheids has been only marginally investigated, since till a few years ago iron measurements for these objects were not available. As we have already mentioned in §2, Walraven *VBLUW* photometry is available for more than 160 Galactic Cepheids. The pulsation properties of these objects will be discussed in a forthcoming paper (Pedicelli et al. 2010). Interestingly, three out of the four target Cepheids belong to this sample, namely AV Sgr, UZ Sct and VY Sgr. For these Cepheids were secured at least 30 phase points in five-

Table 4. Intrinsic parameters and iron abundances for the target Cepheids.

Name	$T_{\rm eff}$(LDR)	log g	$v_{\rm t}$	$T_{\rm eff}$(Model)	[Fe I/H]	[Fe II/H]	<[Fe/H]>	[Fe/H]$_{And}$
V340 Ara	5425±146	0.2	3.5	5475	0.38±0.17	0.42±0.26	+0.40±0.21	+0.31±0.10
UZ Sct	4790±95	0.6	3.7	4850	0.35±0.17	0.35±0.27	+0.35±0.21	+0.33±0.10
AV Sgr	5407±53	0.9	4.2	5450	0.26±0.12	0.28±0.12	+0.27±0.12	+0.34±0.10
VY Sgr	5268±146	1.0	3.2	5400	0.38±0.17	0.36±0.26	+0.35±0.21	+0.26±0.10

VBLUW bands that properly cover the entire pulsation cycle. The intrinsic accuracy of individual measurements is of the order of a few millimag. The uncertainty on the mean magnitudes, estimated using a fit with a cubic spline, is at most of the order of a few hundredths of a magnitude. In order to investigate the possible correlation between luminosity amplitude and iron abundance, the Walraven B_W,V_W-band photometric data were transformed into the Johnson B_J,V_J-band data using the relations:

$$V_J = 6.886^{mag} - 2.5\ V_W - 0.1916\ (V-B)_W \quad (4)$$

$$(B-V)_J = 2.7947\ (V-B)_W - 1.2052\ (V-B)_W^2 + 0.6422\ (V-B)_W^3 - 0.0100 \quad (5)$$

Accurate iron abundance measurements for Walraven Cepheids are available for 77 objects, while for 67 objects metallicity estimates are available based on the Walraven metallicity index (Pedicelli et al. 2008, and references therein). This sample was supplemented with 115 Cepheids for which accurate iron abundances exist in the literature, based on high resolution spectra (Andrievsky et al. 2002a,b,c, 2004; Lemasle et al. 2007; Sziládi et al. 2007; Lemasle et al. 2008; Romaniello et al. 2008). We ended up with a sample of 259 Galactic Cepheids and the top panel of Fig. 5 shows the metallicity distribution. In order to provide accurate estimates of the mean metallicity and of the spread in metallicity of the Galactic disk, we ran a Gaussian kernel with a σ equal to the metallicity uncertainty of individual Cepheids. The metallicity distribution we obtained is plotted in the bottom panel of Fig. 5 and the red line shows the Gaussian fit. We found a solar mean metallicity ($< [Fe/H] > \sim$ -0.03) and a sigma of 0.18 dex. These values agree quite well with similar metallicity distributions available in the literature (Chiappini et al. 2001; Cescutti et al. 2007). Our metallicity distribution is also asymmetric, and indeed the metal-poor tail is shallower than the metal-rich one. This finding agrees with predictions based on Galactic chemical evolution models (Holmberg et al. 2007; Yin et al. 2009).

To constrain the dependence of the pulsation properties on the metal content, we adopted the Bailey diagram, i.e. luminosity amplitude vs. pulsation period. Data plotted in Figures 6 and 7 show the V, B luminosity amplitudes of the Cepheid sample adopted by Pedicelli et al. (2009). The amplitudes are based either on Walraven photometry –transformed into the Johnson system (see §2.1)– or on data in the Galactic Cepheid catalog provided by Fernie et al. (1995). To constrain the possible dependence of the pulsation amplitude on the metal content we selected three different sub-samples representative of the metal-poor ([Fe/H]≤-0.30 dex) tail, of the metal-rich ([Fe/H]≥0.13 dex) tail and of the peak metallicity (-0.04 ≤[Fe/H]≤-0.02 dex). The three samples roughly include two dozen of Cepheids. Data plotted in the top panels of Figures 6 and 7 display that both *V* and *B*-band amplitudes are not correlated with the metal content. This feature does not agree with a well established theoretical and empirical evidence of RR Lyrae stars (Bono et al. 2007), i.e. the prototype of low-mass, helium burning radial variables located inside the so-called Cepheid instability strip. Such a difference can be partially explained with the empirical circumstance that Galactic RR Lyrae variables cover almost three dex in metal content, when moving from the halo to the bulge, while Galactic Cepheids in the disk only cover one dex. Moreover, the Hertzsprung progression causes a systematic decrease in the pulsation amplitudes for periods across ten days (Payne-Gaposchkin 1951, 1954). Current empirical (Andreasen & Petersen 1987; Welch et al. 1997; Beaulieu 1998; Moskalik et al. 2000) and theoretical (Bono et al. 2000b) evidence indicates that a decrease in metal content causes a systematic drift in the center of the Hertzsprung progression toward shorter periods. This means a reshuffle in the pattern of the luminosity amplitudes as a function of the pulsation period when dealing with Cepheids with different metal abundances. However, the spread in the amplitudes is also present at periods shorter and longer than the Hertzsprung progression. This indicates that the lack of a well defined correlation with metallicity might also be due to the dependence of the topology of the instability strip on the chemical composition (Pel & Lub 1978; Bono et al. 1999, 2000a) to evolutionary effects and to binarity (see Pedicelli et al. 2010, in preparation).

As a final test concerning the metallicity distribution of Galactic Cepheids we split the sample into short ($\log P \leq 1.0$) and long ($\log P > 1.0$) period objects. Data plotted in the bottom panels of Figures 6 and 7 show that metal-rich ([Fe/H]≥-0.13 dex) Cepheids are more frequent among long- than among short-period Cepheids (15% vs 5%) Cepheids. On the other hand, the metal-poor ([Fe/H]≤-0.30 dex) Cepheids are equally distributed between the two groups. The evidence that the period distribution of classical Cepheids depends on the metal-content dates back to Gascoigne (1974, and references therein), who realized that the peak shifts toward shorter periods when moving from Galactic to Small Magellanic Cloud Cepheids. Subsequent evolutionary tracks for intermediate-mass stars showed that more metal-poor structures are characterized, at fixed mass, by blue loops that cover a larger temperature range. This means that the minimum Cepheid mass crossing the instability strip is smaller in metal-poor that in metal-rich systems. As a consequence a systematic drift in the period distribution of metal-rich Cepheids is expected. However, the period cut we adopted is well beyond the short period cutoff of Galactic Cepheids, thus suggesting that the paucity of metal-rich Cepheids among short-period Cepheids is probably due to an observational bias.

6. Summary and conclusions

We provided accurate BW distances and radii for four metal-rich Cepheids, namely V340 Ara, UZ Sct, AV Sgr and VY Sgr. Current distance estimates, taken at face value, agree quite well with similar estimates based either on empirical (Fouqué et al. 2007) or on theoretical NIR PL relations. However, the uncertainties affecting the BW distances, by summing in quadrature the errors in the fit and the errors estimated with the Monte Carlo

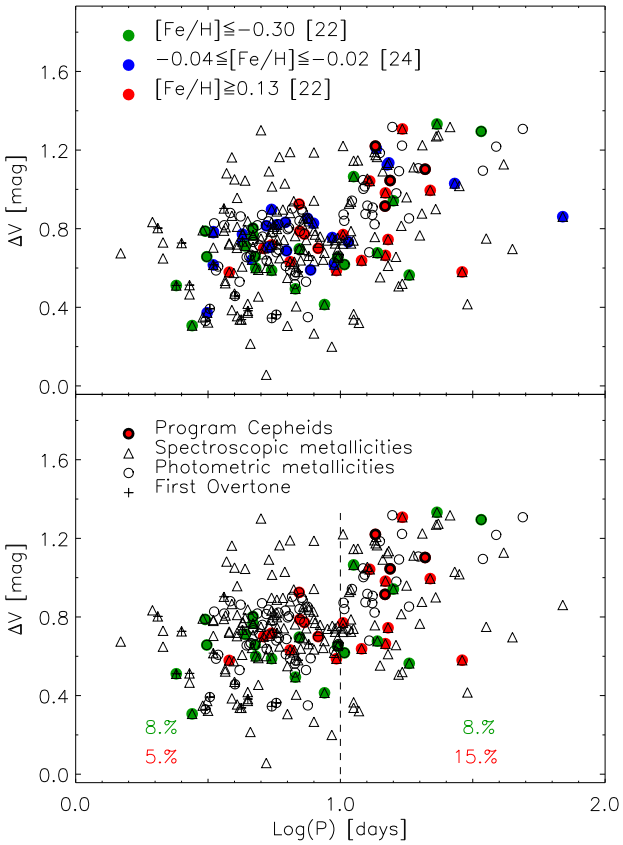

Fig. 6. Top – *V*-band amplitude versus period for a sample of 259 Galactic Cepheids. Triangles and circles display spectroscopic and photometric metallicities, respectively. Red and green dots mark metal-rich ([Fe/H]≥ 0.13) and metal-poor ([Fe/H]≤ -0.30) Cepheids, while the blue ones show Cepheids with iron abundances ranging from -0.04 to -0.02 dex. The selected metal-rich Cepheids are marked with a cross, while the pluses mark first overtone pulsators. Bottom – same as the top, but the vertical dashed line splits short- ($\log(P) \leq 1.0$) and long-period ($\log(P) > 1.0$) Cepheids. The fractions of metal-poor and metal-rich Cepheids are also labeled.

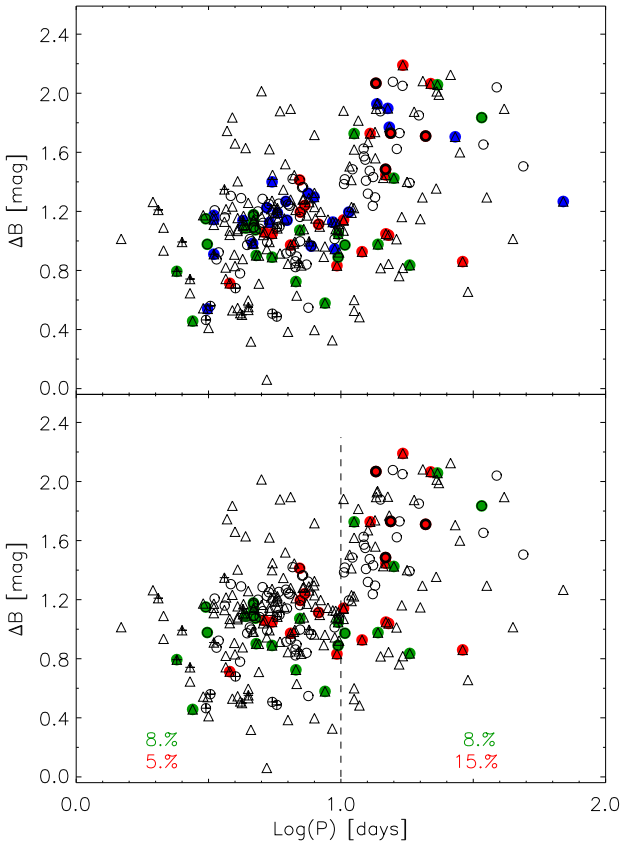

Fig. 7. Same as Figure 6, but for the *B*-band amplitudes.

simulations, are on average a factor of 3-4 smaller than for distances based on predicted and empirical NIR PL relation. The same outcome applies to the mean Cepheid radii, but the uncertainties on the BW radii, by summing in quadrature errors on the fit and errors from Monte Carlo simulations, are on average a factor of two larger than for radii based either on the empirical or on the theoretical PR relation provided by G07 and by Petroni et al. (2003), respectively.

We also collected high-resolution, high signal-to-noise ratio spectra to measure the iron abundances of the target Cepheids. Special attention was paid to provide accurate estimates of intrinsic parameters (effective temperature, surface gravity, microturbulent velocity) directly from observed spectra. We performed detailed measurements of iron abundances using large samples of Fe I and Fe II lines. Current abundances indicate that selected Cepheids are super metal-rich and agree, within 1σ, with iron abundances provided by Andrievsky et al. (2002b) using a similar approach.

We adopted a sample of 259 Galactic Cepheids for which are available either spectroscopic iron measurements or metallicity estimates based on the Walraven metallicity index (Pedicelli et al. 2008). We found that classical Cepheids do not seem to show in the Bailey diagram (luminosity amplitude vs pulsation period), in contrast with low-mass helium burning RR Lyrae stars, a clear correlation between luminosity amplitude and metallicity. The lack of such a correlation might be the consequence of the Hertzsprung progression. We also found that a good fraction of metal-rich ([Fe/H]≥0.13 dex) Cepheids are located among long-period ($\log P \geq 1.0$) variables. However, for the moment this can only be considered as circumstantial evidence, since the current sample is probably affected by selection bias. Metal-rich Cepheids are located in the inner disk and are typically affected by large extinctions. The selected Cepheids have Galactocentric distances smaller than 6.5 kpc and their reddening ranges from 0.6 to 1.3 mag. Detailed analysis concerning the pulsation properties of metal-rich Cepheids best awaits more complete samples. However, the game is worth the candle, since classical Cepheids are excellent tracers of young stellar populations. Their pulsation properties and their radial distribution across the inner Galactic disk and the bar can provide robust constraints on the bar-driven formation scenario (van Loon et al. 2003; Debattista et al. 2004; Zoccali et al. 2006) on short (10-100 Myr) timescales.

Acknowledgements. We acknowledge an anonymous referee for his/her positive opinion concerning the content of this investigation. Two of us (SP, GB) acknowledge ESO support (DGDF funds) for a stay in Garching, during which a good part of this paper was written. It is a pleasure to thank M. Zoccali for interesting discussions concerning the interaction between the Galactic disk and the bulge. We also thank G. Iannicola and I. Ferraro for their suggestions concerning Gaussian smoothing.

References

Andreasen, G. K. & Petersen, J. O. 1987, A&A, 180, 129
Andrievsky, S. M., Bersier, D., Kovtyukh, V. V., et al. 2002a, A&A, 384, 140
Andrievsky, S. M., Kovtyukh, V. V., Luck, R. E., et al. 2002b, A&A, 381, 32
Andrievsky, S. M., Kovtyukh, V. V., Luck, R. E., et al. 2002c, A&A, 392, 491
Andrievsky, S. M., Luck, R. E., Martin, P., & Lépine, J. R. D. 2004, A&A, 413, 159
Baade, W. 1926, Astronomische Nachrichten, 228, 359
Barnes, T. G., Evans, D. S., & Parsons, S. B. 1976, MNRAS, 174, 503
Barnes, III, T. G., Jefferys, W. H., Berger, J. O., et al. 2003, ApJ, 592, 539
Beaulieu, J. P. 1998, Memorie della Societa Astronomica Italiana, 69, 21
Benedict, G. F., McArthur, B. E., Feast, M. W., et al. 2007, AJ, 133, 1810
Berdnikov, L. N. 1992, Astronomical and Astrophysical Transactions, 2, 107
Bersier, D., Burki, G., & Kurucz, R. L. 1997, A&A, 320, 228
Bono, G., Caputo, F., & Di Criscienzo, M. 2007, A&A, 476, 779
Bono, G., Caputo, F., Fiorentino, G., Marconi, M., & Musella, I. 2008, ApJ, 684, 102
Bono, G., Castellani, V., & Marconi, M. 2000a, ApJ, 529, 293
Bono, G., Marconi, M., & Stellingwerf, R. F. 1999, ApJS, 122, 167
Bono, G., Marconi, M., & Stellingwerf, R. F. 2000b, A&A, 360, 245
Cescutti, G., Matteucci, F., François, P., & Chiappini, C. 2007, A&A, 462, 943
Chiappini, C., Matteucci, F., & Romano, D. 2001, ApJ, 554, 1044
Debattista, V. P., Carollo, C. M., Mayer, L., & Moore, B. 2004, ApJ, 604, L93
di Benedetto, G. P. 2008, MNRAS, 390, 1762
Feast, M. 1999, PASP, 111, 775
Fernie, J. D., Evans, N. R., Beattie, B., & Seager, S. 1995, Information Bulletin on Variable Stars, 4148, 1
Fouqué, P., Arriagada, P., Storm, J., et al. 2007, A&A, 476, 73
Fouqué, P. & Gieren, W. P. 1997, A&A, 320, 799
François, P., Depagne, E., Hill, V., et al. 2007, A&A, 476, 935
Freedman, W. L., Madore, B. F., Gibson, B. K., et al. 2001, ApJ, 553, 47
Gascoigne, S. C. B. 1974, MNRAS, 166, 25P
Gieren, W., Storm, J., Barnes, III, T. G., et al. 2005, ApJ, 627, 224
Gieren, W. P., Barnes, III, T. G., & Moffett, T. J. 1993, ApJ, 418, 135
Gieren, W. P., Fouqué, P., & Gomez, M. 1998, ApJ, 496, 17
Gieren, W. P., Fouqué, P., & Gomez, M. I. 1997, ApJ, 488, 74
Gray, D. F. 1994, PASP, 106, 1248
Groenewegen, M. A. T. 2004, MNRAS, 353, 903
Groenewegen, M. A. T. 2007, A&A, 474, 975
Groenewegen, M. A. T. 2008, A&A, 488, 25
Holmberg, J., Nordström, B., & Andersen, J. 2007, A&A, 475, 519
Kanbur, S., Marconi, M., Ngeow, C., et al. 2009, in Stellar Pulsation: Challenges for Theory and Observation, Vol. 1170, American Institute of Physics Conference Series, ed. J. A. Guzik & P. A. Bradley, 18–22
Kervella, P., Bersier, D., Mourard, D., et al. 2004a, A&A, 428, 587
Kervella, P., Mérand, A., Szabados, L., et al. 2008, A&A, 480, 167
Kervella, P., Nardetto, N., Bersier, D., Mourard, D., & Coudé du Foresto, V. 2004b, A&A, 416, 941
Kovtyukh, V. V., Andrievsky, S. M., Belik, S. I., & Luck, R. E. 2005, AJ, 129, 433
Kovtyukh, V. V. & Gorlova, N. I. 2000, A&A, 358, 587
Krockenberger, M., Sasselov, D., Noyes, R., et al. 1998, in Cool Stars, Stellar Systems, and the Sun, Vol. 154, Astronomical Society of the Pacific Conference Series, ed. R. A. Donahue & J. A. Bookbinder, 791–+
Laney, C. D. & Stobie, R. S. 1995, MNRAS, 274, 337
Lemasle, B., François, P., Bono, G., et al. 2007, A&A, 467, 283
Lemasle, B., François, P., Piersimoni, A., et al. 2008, A&A, 490, 613
Lub, J. & Pel, J. W. 1975, in IAU Symposium 190, Multicolor Photometry and the Theoretical HR Diagram, 133–134
Lub, J. & Pel, J. W. 1977, A&A, 54, 137
Luck, R. E. & Andrievsky, S. M. 2004, AJ, 128, 343
Maciel, W. J. & Costa, R. D. D. 2009, ArXiv e-prints
Macri, L. M., Stanek, K. Z., Bersier, D., Greenhill, L. J., & Reid, M. J. 2006, ApJ, 652, 1133
Marconi, M. 2009, Memorie della Societa Astronomica Italiana, 80, 141
Marengo, M., Evans, N. R., Barmby, P., Bono, G., & Welch, D. 2009, in The Evolving ISM in the Milky Way and Nearby Galaxies
Marengo, M., Karovska, M., Sasselov, D. D., et al. 2003, ApJ, 589, 968
Mérand, A., Kervella, P., Coudé Du Foresto, V., et al. 2005, A&A, 438, L9
Moskalik, P., Krzyt, T., Gorynya, N. A., & Samus, N. N. 2000, in Astronomical Society of the Pacific Conference Series, Vol. 203, IAU Colloq. 176: The Impact of Large-Scale Surveys on Pulsating Star Research, ed. L. Szabados & D. Kurtz, 233–234
Nardetto, N., Fokin, A., Mourard, D., et al. 2004, A&A, 428, 131
Nardetto, N., Gieren, W., Kervella, P., et al. 2009, A&A, 502, 951
Nardetto, N., Mourard, D., Mathias, P., Fokin, A., & Gillet, D. 2007, A&A, 471, 661
Payne-Gaposchkin, C. 1951, Astrophysics: A Topical Symposium, New York: McGraw Hill, 495
Payne-Gaposchkin, C. 1954, Annals of Harvard College Observatory, 113, 153
Pedicelli, S., Bono, G., Lemasle, B., et al. 2009, A&A, 504, 81
Pedicelli, S., Lub, J., Pel, J. W., et al. 2008, Memorie della Societa Astronomica Italiana, 79, 539
Pel, J. W. 1976, A&AS, 24, 413
Pel, J. W. & Lub, J. 1978, in IAU Symposium, Vol. 80, The HR Diagram - The 100th Anniversary of Henry Norris Russell, ed. A. G. D. Philip & D. S. Hayes, 229–236
Petroni, S., Bono, G., Marconi, M., & Stellingwerf, R. F. 2003, ApJ, 599, 522
Romaniello, M., Primas, F., Mottini, M., et al. 2008, A&A, 488, 731
Sandage, A., Tammann, G. A., & Reindl, B. 2009, A&A, 493, 471
Scowcroft, V., Bersier, D., Mould, J. R., & Wood, P. R. 2009, MNRAS, 396, 1287
Storm, J., Carney, B. W., Gieren, W. P., et al. 2004, A&A, 415, 531
Sziládi, K., Vinkó, J., Poretti, E., Szabados, L., & Kun, M. 2007, A&A, 473, 579
Tammann, G. A., Sandage, A., & Reindl, B. 2003, A&A, 404, 423
van Leeuwen, F. 2007, A&A, 474, 653
van Leeuwen, F., Feast, M. W., Whitelock, P. A., & Laney, C. D. 2007, MNRAS, 379, 723
van Loon, J. T., Gilmore, G. F., Omont, A., et al. 2003, MNRAS, 338, 857
Walraven, J. H., Tinbergen, J., & Walraven, T. 1964, Bull. Astron. Inst. Netherlands, 17, 520
Welch, D. L., Alcock, C., Allsman, R. A., et al. 1997, in Variables Stars and the Astrophysical Returns of the Microlensing Surveys, ed. R. Ferlet, J.-P. Maillard, & B. Raban, 205–+
Wesselink, A. J. 1946, Bull. Astron. Inst. Netherlands, 10, 91
Yin, J., Hou, J. L., Prantzos, N., et al. 2009, A&A, 505, 497
Zoccali, M., Lecureur, A., Barbuy, B., et al. 2006, A&A, 457, L1